Soft fluidic rotary actuator with improved actuation properties

J. Fras[1], Y. Noh[2], H. Wurdemann[3], K. Althoefer[1]

***Abstract*— The constantly increasing amount of machines operating in the vicinity of humans makes it necessary to rethink the design approach for such machines to ensure that they are safe when interacting with humans. Traditional mechanisms are rigid and heavy and as such considered unsuitable, even dangerous when a controlled physical contact with humans is desired. A huge improvement in terms of safe human-robot interaction has been achieved by a radically new approach to robotics - soft material robotics. These new robots are made of compliant materials that render them safe when compared to the conventional rigid-link robots. This undeniable advantage of compliance and softness is paired with a number of drawbacks. One of them is that a complex and sophisticated controller is required to move a soft robot into the desired positions or along a desired trajectory, especially with external forces being present. In this paper we propose an improved soft fluidic rotary actuator composed of silicone rubber and fiber-based reinforcement. The actuator is cheap and easily manufactured providing near linear actuation properties when compared to pneumatic actuators presented elsewhere. The paper presents the actuator design, manufacturing process and a mathematical model of the actuator behavior as well as an experimental validation of the model. Four different actuator types are compared including a square-shaped and three differently reinforced cylindrical actuators.**

I. INTRODUCTION

A large range of actuators have been employed in various areas such as robot hands, surgical robots, hybrid assistive limb systems, and prosthetic limbs and hands. The traditional approach of designing mechanical systems is focused on making use of electrical actuators joined with transmission mechanisms such as gears or linear translation systems to transmit high torque to mechanical joints or to convert rotational motion to translational motion - in such cases, the overall system is heavy and bulky.

As the number of machines operating in the vicinity of humans is growing, the risk of potentially harmful human-machine interaction is increasing, and, hence, there is a need of redesign in robotics with safety being at the forefront of considerations. Improving robotics safety is still an ongoing process also in the area of traditional actuator mechanics. With current advances in technology, actuators get smaller and lighter, sophisticated sensing is incorporated into their structure and new control strategies are being developed [1]. However, this approach is not perfect as accidents still happen, and the impact of a rigid device can still exceed a safety threshold.

The risk of injury is significantly decreased by a radically new robotics approach, soft material robotics [2]–[4]. Thanks to soft and compliant materials that these robots are composed of, a significantly safer interaction with humans compared to conventional rigid-link robots can be achieved. However, the biggest soft robotics advantage, i.e. softness and compliance, brings also a number of drawbacks. One of them is that actuation and control becomes very complex and demanding since the actuators and linkages are made of soft and compliant materials. One of the most popular soft actuators are flexible fluidic actuators (FFA). There are different types of FFAs [5] that can be classified by their behavior e.g., actuators that contract along their primary axis, those that expand along their primary axis, those that twist along their primary axis (rotating) [6], those that bend (also rotation) [7]–[10], and those with complex motion behaviors [11], [12].

The rotary FFAs presented here get their ability to ratate from their particular geometry; they can be used to provide rotational movement between two robotics links [5], [13]–[15]. In [13], a soft rotary actuator is presented consisting of a hollow silicone rubber reinforced by nylon fibers so that the device expands predominantly in the circumferential direction when pressurized. In [15], a similar actuator is proposed but reinforced with unstretchable fabric layers instead of the fiber. Despite the reinforcement those actuators not only bend but also deform in radial direction when pressurized. The effect is caused by the geometrical configuration of the device and the reinforcement density. Such an effect makes the actuator extend and influences its behavior in a way that it improves linearity. In this paper, we are proposing

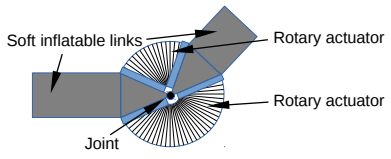

Fig. 1: An entirely soft robotic arm driven by the soft fluidic rotary actuator.

an improved soft actuator using silicon rubber reinforced with polyester fibers specifically tailored to achieve rotary motion. The actuator is designed to be used in a robotic arm combined with soft stiffness-controllable robot links [16] as presented in Figure 1. As the actuator is designed to drive a robotic arm any nonlinear behavior is highly

[1]J. Fras and K. Althoefer are with the Centre of Advanced Robotics @ Queen Mary (ARQ), Faculty of Science and Engineering, Queen Mary University of London, London E1 4NS, UK j.fras@qmul.ac.uk, k.althoefer@qmul.ac.uk

[2]Y. Noh is with the Department of Informatics, King's College London, London WC2R 2 LS, UK yohan.noh@kcl.ac.uk

[3]H.A. Wurdemann is with the Department of Mechanical Engineering, University College London, London WC1E 6BT, UK h.wurdemann@ucl.ac.uk

undesired since that would require more complicate control. Any radial deformation or expansion of the actuator may be a problem too, as it makes the arm dimensions unstable and increases the risk of self-collision or uncontrolled interaction with the environment. The modified reinforcement strategy and circular cross-section shape solve the shortcomings of conventional rotary actuators. The proposed design shows not only highly linear characteristics, but also reduces the radial expansion observed in other designs.

II. MECHANICAL DESIGN

The actuator is composed of three main parts: an actuation chamber, a tip and a base. The actuation chamber is made of soft silicone EcoFlex 0050 (Shore 00-50), while for the base and the tip the relatively stiff silicone - SmoothSill 940 (Shore 40 A)- has been used. The chosen materials allow the actuator to bend and prevent its both ends from deformation. The actuation chamber is reinforced with a polyester thread that restrains its radial expansion. The application of the thread for such a purpose has been already extensively examined and shows very good performance [17], [8]. The thread is formed in a helix with an equally spaced pitch along the actuator angular length. The intersection of all the planes that the circular cross sections of the helix are located on defines the actuator rotation axis. The complete actuator weighs around 20 grams. The actuator design is presented in Figure 2.

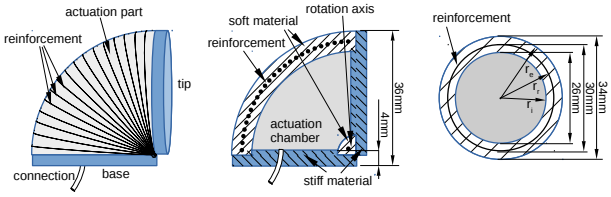

(a) (b) (c)

Fig. 2: Single module design. a) side view, b) side cross-section, c) front cross-section.

A. Cross-section and reinforcement geometry

For the proposed actuator a circular shape of the cross-section has been chosen, as the circular cross-section shape is the only shape that does not change its geometry during the actuation. Any other cross-section shapes (e.g. rectangular, elliptical, etc) would change and converge towards the circular shape when pressurized, Figure 3b. Such a deformation results in the change of the cross-section area and influences its geometrical center position. This, in turn, affects the actuator characteristics rendering it less linear. The deformation towards a circular shape of an actuator with a non-circular cross-section when pressurized is illustrated in Figure 3. Its impact on the actuation process is further discussed in Sections III and IV.

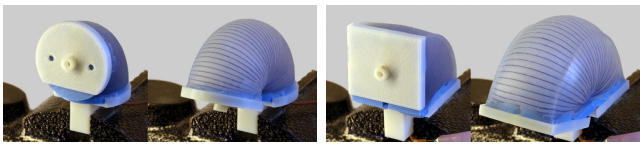

(a) (b)

Fig. 3: Deformation of the actuator cross-section geometry when pressurized: a) circular cross-section - preservation of circular shape, b) square cross-section - deformation from square shape (non pressurized) to circular shape (pressurized).

B. Fiber Reinforcement

The number of turns of the helical reinforcement structure (angular density) does also affect the mechanical properties of the actuator. Although the flexible actuator body is constrained by the thread, it can still expand between the reinforcement thread (ballooning effect). This also affects the cross-section area and its geometrical center position. The distance between the turns of the thread increases during actuation as the actuator stretches along its axis - hence, the spacing between the turns becomes more significant and ballooning may occur (Figure 4).

The perfect solution would be reaching an infinitesimal thread-to-thread angular distance, but in a real implementation of the concept, this is unachievable. Actuator deformation related to the number of turns / pitch of the reinforcement fiber is shown in Figure 4.

(a) (b) (c)

Fig. 4: The actuator cross-section changes when pressurized. The more dense the reinforcement, the less deformation is observed. Different angular densities compared: a) $1/18^o$, b) $1/15^o$, c) $1/2.25^o$. Different pressure values for each actuator, see section IV.

C. Fabrication

The actuator manufacturing process consists of several steps. The first step is the reinforcement shaping using a dedicated three-part core (Figure 5a). The core has an embedded structure that helps keeping the thread in place. The core consists of three parts that can be separated easily and, thus, facilitates the core's removal after the molding process is complete. Once the core is wrapped with the thread it is covered with soft silicone in the second step (Figure 5b). For that manufacturing step another, external two-part mold is used. After the silicone is cured the external mold is opened and the three-part core is gently removed

from the silicon layer, while the thread remains embedded in the silicone. In the third step, the internal layer of the actuation part is created by filling it with the next portion of silicone and putting another, smaller core inside. After that the actuation chamber is closed by creating a round cap of stiff silicone using another mold, Figure 5c. It is noted that all mold parts are 3d printed.

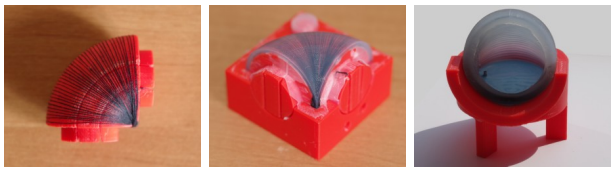

(a) (b) (c)

Fig. 5: Manufacturing process: a) reinforcement deployment, b) external layer of active part molding, c) closing both ends of the actuator.

III. MATHEMATICAL DESCRIPTION

Nowadays almost any mechanical object can be described by a numerical function and its behavior can be modeled using finite element methods. Such a solution, however, is computationally complex and requires a precise object description. Thus we propose a simplified static mathematical model that requires only a small set of calculations and is based on a number of assumptions. We assume that the cross-section geometry in any plane parallel to the actuator rotation axis remains constant during actuation - this is assured by the fiber reinforcement. We also assume that there is no deformation of the base and the tip of the actuator. The fiber thread is considered to only limit the radial expansion - all other effects of the fiber onto the robot structure have been neglected as there was no such impact observed in cases of similar silicone structures [8].

A. General model

Consider an actuation bending moment resulting from the pressure inside the actuation chamber as M_p. In an equilibrium the actuation bending moment is balanced by stress in the actuator body M_I and the generated torque τ. (1), Figure 6c:

$$M_p = \tau + M_I \tag{1}$$

The bending moment inside the actuation chamber is generated by the pressure acting on the tip and on the base of the actuator. Assuming that the base is fixed, the impact of the pressure acting on it can be omitted. Since the pressure acting on the actuator walls other than base and tip does not cause any displacement it can be ignored as well. The bending moment acting on the tip related to the rotation axis can be expressed as (2):

$$M_p = \int_A pxda = p\int_A xda \tag{2}$$

where A corresponds to the internal tip wall area, p denotes the pressure acting and x stands for the distance of da from the rotation axis (Figure 6a). As the pressure has a constant value inside the chamber the p variable can be taken outside the integral.

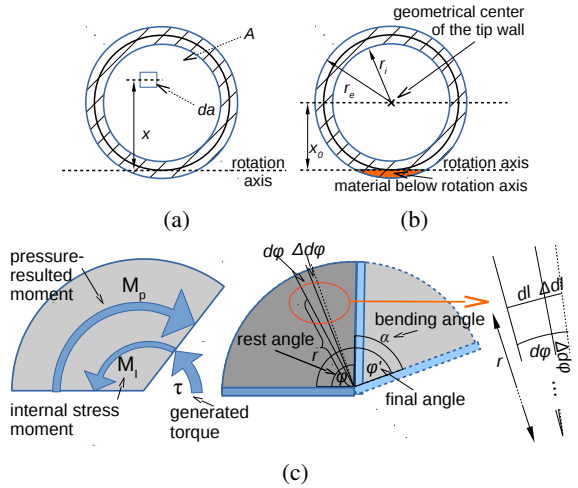

Fig. 6: Mathematical description of the actuator behavior, a), b) front view, tip wall of the actuation chamber, c) side view

Introducing a x_0 variable being the distance from rotation axis to the tip's geometrical center (Figure 6b), the integral can be written as (3)

$$M_p = p\int_A (x - x_0 + x_0)da = p\left(\int_A (x - x_0)da + \int_A x_0 da\right) \tag{3}$$

Considering (3) and (4) , the bending moment is equal to (5).

$$\int_A (x - x_0)da = 0, \int_A x_0 da = Ax_0 \tag{4}$$

$$M_p = pAx_0 = px_0\pi r_i^2 \tag{5}$$

Using the same justification as for pressure related to actuation moment, the internal stress moment can be calculated as:

$$M_I = \sigma x_0 A_b = \sigma x_0 \pi(r_e^2 - r_i^2) \tag{6}$$

where A_b denotes the area of the actuator body in the cross-section.

Putting all the equations together we get (7):

$$\tau = px_0\pi r_i^2 - \sigma x_0 \pi(r_e^2 - r_i^2). \tag{7}$$

The stress variable σ depends on the material properties and its deformation value ϵ. It can be read form the stress-strain curve of EcoFlex 0050 material used for the actuator body. The curve has been measured and is presented in Figure 7. The strain ϵ at a certain point corresponding to actuation angle α can be expressed as:

$$\epsilon = \frac{\Delta dl}{dl} = \frac{r\Delta d\varphi}{rd\varphi} = \frac{\varphi' - \varphi}{\varphi} = \frac{\alpha}{\varphi}. \quad (8)$$

where φ and φ' stand for the actuator's rest and active angles, respectively (Figure 6c).

It is important to note that the strain does not depend on the r value and remains constant for the entire actuator volume (despite a small part of the flexible actuation chamber below the rotation axis that has been neglected due to its relatively small volume - marked in orange in Figure 6b.

With regards to the measured characteristics (7) can be rewritten as:

$$\tau(p, \alpha) = px_0\pi r_i^2 - \sigma(\epsilon(\alpha))x_0\pi(r_e^2 - r_i^2). \quad (9)$$

For a constant angle α the torque is a linear function of pressure $\tau(p, \alpha = \alpha_0) = px_0\pi r_i^2 - c_{\alpha_0}$ since the last part of the equation is constant in such case.

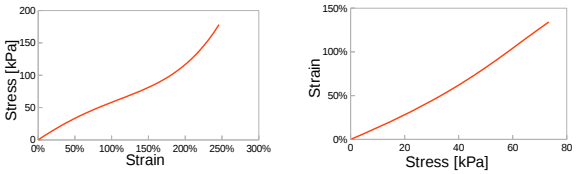

(a) (b)

Fig. 7: Relation between strain and stress of Ecoflex 0050, a) stress-strain curve, b) inverted relationship for around 100% deformation (the range of the tested actuator motion).

From (8) the actuation angle α can be expressed as $\alpha = \varphi\epsilon$, where ϵ depends on the pressure p and the load τ:

$$\alpha(p, \tau) = \varphi\epsilon(\sigma(p, \tau)),$$
$$where : \sigma(p, \tau) = \frac{px_0\pi r_i^2 - \tau}{x_0\pi(r_e^2 - r_i^2)}. \quad (10)$$

The final bending angle equation contains the strain ϵ as a function of stress, which is a linear a function of pressure for constant torque. Thus, for a constant torque the actuation angle should reflect the inverse stress-strain curve (Figure 7b).

IV. EXPERIMENTS AND VALIDATION

In this section the experimental setup and assumed model validation process is described. The results are discussed. For the trials the actuator was powered by pressurized air from a pressure tank.

A. Bending characterization

For this test the experimental setup was composed of a pressure source, a pressure indicator, a camera and our examined rotary actuator. The actuator was equipped with a lightweight rod attached to its free end in order to determine its momentary configuration. (It is noted that a vision system trained on the lightweight rod was used to obtain real-time data on the movement of the actuator.) Our rotary actuator was connected to a pressure source through a proportional throttle that was adjusted to pass the actuation gas slowly so the actuation process was very slow and steady. High-speed actuation was not investigated here because, in such a case, the dynamics of the system cannot be neglected, and the pressure measured at the pressure pipe providing the fluid to the device would differ from the actual pressure in the actuation chamber due to the dynamic pressure distribution in the system (described by Darcy–Weisbach equation).

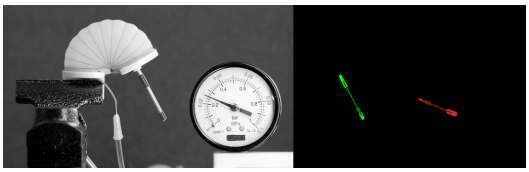

Fig. 8: Single frame of a recorded sequence, bending angle and pressure indicators detected (green and red consequently)

The whole process was recorded with a camera and then using image processing, both the pressure and the bending angle were determined in the frames of the recorded video. A single frame of the data and the image processed are presented in Figure 8.

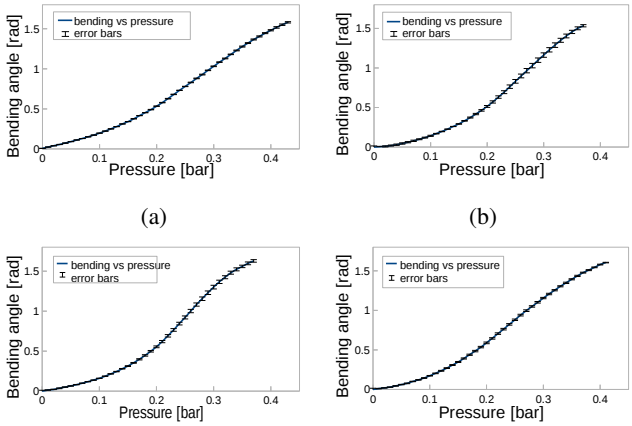

(a) (b)

(c) (d)

Fig. 9: Bending angle vs pressure with error bars. Results for 0 degree actuation angle and different actuators regarding its cross-section shape and angular distance between reinforcement cycles: a) circular, 2.25^o, b) circular, 15^o, c) circular, 18^o, d) square, 2.25^o.

In this experimental study, four different actuators have been examined. Three of them have had circular cross-sections and one had a rectangular one. The cylindrical ones were identical apart from the fact that their reinforcement had different numbers of turns - with 2.25^o, 15^o and 18^o of spacing. The square-shaped actuator had similar dimensions and was reinforced with 2.25^o of spacing. All the prototype actuators had a 90^o passive angle. The circular circumference actuators had a 26mm internal and a 34mm external diameter, rectangular cross-section actuators had 26mm and 34mm

internal and external sides length, respectively. In all the cases the reinforcement was embedded in the middle of the silicone layer.

Each actuator was actuated 6 times with exactly the same pressure increase speed. Each actuator was actuated in the range from 0 to 90^o.

The plots of the bending angle as a function of pressure with statistical errors included are presented in Figure 9. As can be noticed, none of the tested actuators characteristics is linear and all of them reflect a presumed elastomer strain-stress curve (Figure 7).

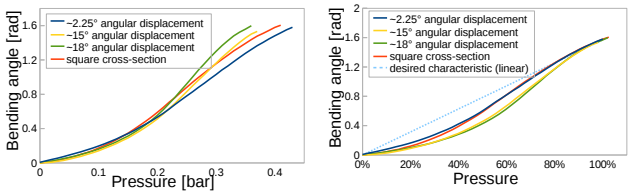

(a) (b)

Fig. 10: Bending angle vs pressure. a) real data, b) the $x-$axis has been normalized for comparison purpose.

In Figure 10, all the curves are presented in the same plot for comparison purposes. On the left hand side all the curves are plotted with respect to the real pressure data. On the right hand side the pressure has been normalized with regards to the 90^o bending angle limit. The desired linear characteristic has been also presented. Such a unification makes it clearly visible that the circular actuator reinforced with the least spacing presents the most linear characteristics. It is interesting to note that the square actuator behaves in a way very similar to the circular one (Figure 10b, red and dark blue lines consequently). The only difference lies in the initial part of the actuation curve. This is because the rectangular shape of the cross-section converges to a circle when pressurized. Thus for higher pressures, when its cross-section is almost circular, the actuator presents the same actuation properties as a circular one.

The actuator characteristics compared to the model is presented in Figure 11. Statistical evaluation of the tested actuator versions is presented in Table I. The statistical evaluation considers a linear characteristic of the same range of motion (0^o - 90^o) and the proposed model for circular actuator cross-section. As expected, the reinforcement density affects the actuator linearity and the more reinforcement cycles, the more linear the actuator is. Since the actuator manufacturing process is highly imprecise, the actual dimensions may vary from assumed. Thus the model prediction may be better if its geometrical parameters (the actuator dimensions) are slightly adjusted. In the last row model prediction errors for adjusted actuator geometry are presented.

B. Torque characterization

A similar setup was used to test for torque in our rotary actuator. In our experiments, pressure was determined in the same way as previously and the torque itself was determined

TABLE I: Bending linearity error for 0-90^o actuation angle.

Actuator geometry, reinforcement spacing	Average deviation from linear characteristic (see Fig. 10b)	Proposed Model Average Error
Circular, 2.25^o	5.8^o	3.2^o
Circular, 15^o	10.6^o	5.3^o
Circular, 18^o	10.6^o	6.6^o
Square, 2.25^o	6.5^o	-
Circular, 2.25^o, Model adjusted	-	1.9^o

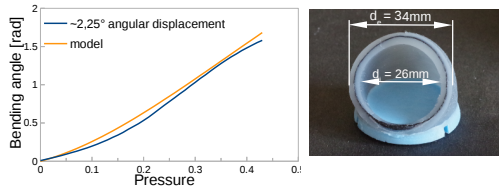

(a) (b)

Fig. 11: a) Bending experimental data aligned with the model prediction, b) the actuator cross-section dimensions.

using a precise electronic scale which was recorded in parallel with the pressure indicator. The actuator was fixed to a hinge that was attached to the scale on the other end (Figure 12a). The growth of the pressure value inside the actuator causes the force to change which is reflected in the scale reading. Knowing the radius of the acting force the torque can be calculated.

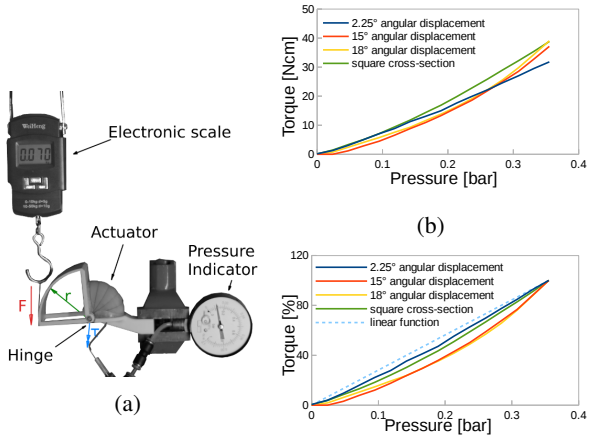

(a) (b) (c)

Fig. 12: Torque characterization; a) setup, b) torque vs pressure, c) all the torque plots combined with torque axis normalized (0 - 100%) for comparison purposes.

The results of the torque measurement at rest actuators angle (0^o) are presented in Figure 13 and a statistical data evaluation is presented in Table II. As expected the highly reinforced actuator with the circular cross-section presents the most linear behavior. All the other actuators are less linear. This effect is related to the cross-section deformation during the pressurization. The cross-section distortion causes its geometry to change, and that makes the torque increase in a nonlinear fashion. All the torque curves are presented in the same plot for comparison, Figure 12b. To make them more

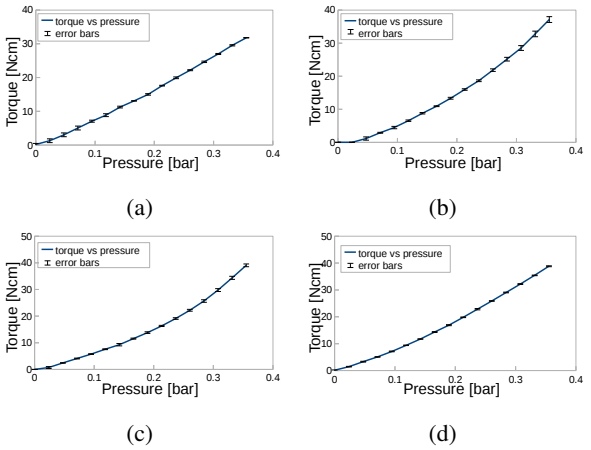

Fig. 13: Torque vs pressure with error bars. Results for different actuators regarding its cross-section shape and angular distance between reinforcement cycles: a) circular, 2.25^o, b) circular, 15^o, c) circular, 18^o, d) square, 2.25^o. Initial configuration of the actuators: 0^o actuation angle.

TABLE II: Torque linearity error for 0 - 0.35bar actuation pressure. Initial actuation angle: 0^o.

Actuator geometry, reinforcement spacing	Average deviation from linear characteristic (see Fig. 12c)	Proposed Model Average Error
Circular, 2.25^o	3.6%	3.8%
Circular, 15^o	12.4%	7.7%
Circular, 18^o	12.1%	6.7%
Square, 2.25^o	6.4%	-

comparable in terms of linearity the torque axis has been normalized for each curve, Figure 12b. As discussed in IV-A, a square-shaped actuator quickly becomes round under the pressure, and this is a suspected reason for the higher torque it provides when compered to similarly reinforced circular one. For the tested dimensions (length of the square cross-section equal to diameter of the circular one) the active cross-section area was approximately 27% bigger when passive and approx. 62% when pressurized in the square-shaped actuator than in circular one.

V. CONCLUSION

In this paper we presented a soft pneumatically-actuated rotary actuator made of silicon rubber reinforced with a polyester fiber. Owing to the actuator compliance, flexibility, achievable angles and generated torque range, it shows to be a promising approach with a wide range of applicability in a variety of domains. Since its body is entirely soft it can be successfully embedded in applications requiring a safe human-machine interaction. The proposed actuator was tested in terms of bending and torque capabilities and compared to a set of similar devices. We have shown that it presents a more linear behavior during actuation when compared to both rectangular and sparsely reinforced actuators even though all the other parameters remained very similar. The average actuation angle difference from an ideal actuator of the same range and completely linear characteristics is around 6^o with the standard deviation around 7^o. The measured torque deviates less than 4% in average from the behavior of the ideal actuator. Improved linearity has been achieved by constraining undesirable effects such as change of cross-section geometry or size.

We have provided an example and justified a hypothesis that the circular actuator's cross-section shape is the preferred one. We have also validated the hypothesis that an increase of the number of turns of the reinforcement fiber improves the actuator behavior.

A mathematical description of the discussed actuator has been proposed and the gathered data appears as expected by the model. The predicted bending angle differs less than 2^o from the experimental data in average and its standard deviation is equal to 2.2^o.

REFERENCES

[1] M. Zinn, O. Khatib, B. Roth, and J. K. Salisbury. Playing it safe [human-friendly robots]. *IEEE Robotics Automation Magazine*, 11(2):12–21, June 2004.

[2] Carmel Majidi. Soft robotics: a perspective—current trends and prospects for the future. *Soft Robotics*, 1(1):5–11, 2014.

[3] Ellen T Roche, Markus A. Horvath, Ali A. Nodeh, Kevin C. Galloway, et al. Design and fabrication of a soft robotic direct cardiac compression device. In *IDETC/CIE*, Boston, MA, 2015. ASME.

[4] B. Mosadegh, P. Polygerinos, C. Keplinger, S. Wennstedt, et al. Pneumatic networks for soft robotics that actuate rapidly. *Advanced Functional Materials*, 24(15):2163–2170, 2014.

[5] A. De Greef, P. Lambert, and A. Delchambre. Towards flexible medical instruments: Review of flexible fluidic actuators. *Precision engineering*, 33(4):311–321, 2009.

[6] Henry M Paynter. Low-cost pneumatic arthrobots powered by tug-and-twist polymer actuators. In *Proc. Japan-USA Symp. on Flexible Automation*, volume 1, pages 107–110, 1996.

[7] J. Fraś, M. Maciaś, F. Czubaczyński, P. Sałek, and J. Główka. Soft flexible gripper design, characterization and application. In *International Conference SCIT, Warsaw, Poland*. Springer, 2016.

[8] J. Fraś, J. Czarnowski, M. Maciaś, J. Główka, M. Cianchetti, and A. Menciassi. New stiff-flop module construction idea for improved actuation and sensing. In *International Conference on Robotics and Automation*, pages 2901–2906. IEEE, 2015.

[9] A. Arezzo, Y. Mintz, M. E. Allaix, S. Arolfo, M. Bonino, G. Gerboni, M. Brancadoro, et al. Total mesorectal excision using a soft and flexible robotic arm: a feasibility study in cadaver models. *Surgical Endoscopy*, pages 1–10, 2016.

[10] K. Suzumori, S. Iikura, and H. Tanaka. Development of flexible microactuator and its applications to robotic mechanisms. In *International Conference on Robotics and Automation*, pages 1622–1627. IEEE, 1991.

[11] A. Stilli, H. A Wurdemann, and K. Althoefer. Shrinkable, stiffness-controllable soft manipulator based on a bio-inspired antagonistic actuation principle. In *International Conference on Intelligent Robots and Systems*, pages 2476–2481. IEEE, 2014.

[12] Satoshi Konishi, Fumie Kawai, and Pierre Cusin. Thin flexible end-effector using pneumatic balloon actuator. *Sensors and Actuators A: Physical*, 89(1):28–35, 2001.

[13] T. Noritsugu, M. Ku Ota, and S. Yoshimatsu. Development of Pneumatic Rotary Soft Actuator. *Transactions of the Japan Society of Mechanical Engineers Series C*, 66(647):2280–2285, 2000.

[14] Qinghua Yang, Libin Zhang, Guanjun Bao, Sheng Xu, and Jian Ruan. Research on novel flexible pneumatic actuator fpa. In *Conference on Robotics, Automation and Mechatronics*, volume 1, pages 385–389. IEEE, 2004.

[15] Y. Sun, Y. S. Song, and J. Paik. Characterization of silicone rubber based soft pneumatic actuators. In *International Conference on Intelligent Robots and Systems*, pages 4446–4453, Nov 2013.

[16] A. Stilli, H. A Wurdemann, and K. Althoefer. A novel concept for safe, stiffness-controllable robot links. *Soft Robotics*.

[17] S. Hirai, P. Cusin, H. Tanigawa, T. Masui, S. Konishi, and S. Kawamura. Qualitative synthesis of deformable cylindrical actuators through constraint topology. In *International Conference on Intelligent Robots and Systems*, pages 197–202 vol.1, 2000.